Nonmagnetic impurity effect in vortex states of chiral superconductors

Takahiro Ueda,[1] Yasuaki Sera,[1] Hiroto Adachi,[1,2] and Masanori Ichioka[1,2]
[1]*Department of Physics, Okayama University, Okayama 700-8530, Japan*
[2]*Research Institute for Interdisciplinary Science, Okayama University, Okayama 700-8530, Japan*

(Received 1 September 2020; revised 11 December 2020; accepted 23 December 2020; published 8 January 2021)

Nonmagnetic impurity scattering effects in the vortex states are studied in the Born and the unitary limits for chiral superconductors by Eilenberger theory. We compare the spatial structure of the pair potential and local electronic structure in chiral p-wave superconductors with those in two types of chiral d-wave superconductors; $d_{1\pm} \equiv d_{xz} \pm id_{yz}$ and $d_{2\pm} \equiv d_{x^2-y^2} \pm id_{xy}$ pairing. Similar behaviors of the pair potentials are seen in $p_\pm$- and $d_{1\pm}$-wave superconductors. In chiral d-wave superconductors, due to lack of Majorana properties relating to the s-wave Cooper pair amplitude, zero-energy vortex bound states are easily destroyed by the impurity scattering, compared to the Born limit in the chiral p_--wave superconductors. This decay is also seen in the unitary limit in the chiral p_--wave superconductors. These differences are also discussed in the relation to s-wave Cooper pair amplitude and the local scattering rate. The impurity effects are also compared with those in s-wave superconductors.

DOI: 10.1103/PhysRevB.103.014506

I. INTRODUCTION

In unconventional superconductors, anisotropic pairing such as p-, d-, and f-wave symmetries are realized. Among them, chiral p-wave and d-wave superconductors have exotic properties, because the time-reversal symmetry is broken due to finite angular momentum L_z of Cooper pair. Chiral p-wave superconductivity is established as a pairing state of the A phase in superfluid ^{3}He [1]. In solid states, one of candidates for the chiral superconductor is Sr_2RuO_4 [2,3]. There, the time reversal symmetry breaking was suggested by experiments of μSR [4] and magneto-optic Kerr effect [5]. While the pairing symmetry has been considered as a spin-triplet chiral p-wave pairing [2,3,6,7], a recent NMR experiment observing Knight shift suggests that the spin-singlet pairing is realized in Sr_2RuO_4 [8,9]. Thus, in addition to the chiral p-wave superconductor of $p_\pm \equiv p_x \pm ip_y$ with $L_z = \pm 1$, we have to examine possibilities of chiral d-wave superconductors, such as $d_{1\pm} \equiv d_{xz} \pm id_{yz}$ with $L_z = \pm 1$ and $d_{2\pm} \equiv d_{x^2-y^2} \pm id_{xy}$ with $L_z = \pm 2$. As other candidate materials, chiral p or f-wave superconductivities are suggested in heavy fermion superconductors UPt_3 [10–12] and UTe_2 [13]. Chiral d-wave pairing is discussed in studies of superconductivity in URu_2Si_2 [14] and SrPtAs [15,16].

In type-II superconductors, by penetration of magnetic fields as quantized flux lines, vortex states appear under applied fields between upper and lower critical fields. Complex value of the superconducting pair potential has the phase winding 2π around a vortex, and the amplitude of the pair potential vanishes at the vortex center. At the vortex core, there exist low energy bound states called Caroli-de Gennes Matricon states [17–19]. The local electronic structure in the vortex bound state is experimentally observed by the scanning tunneling microscope (STM) experiments [20–24]. From the local density of states (LDOS) around a vortex, we can obtain important features of the anisotropic superconductivity. In the direction where the LDOS extends far from the vortex center, pairing function has a node or gap-minimum on the Fermi surface [25–30]. Reflecting the anisotropic gap, the star-shaped vortex core images are observed by STM experiments in $NbSe_2$ [21,29,30] and YNi_2B_2C [31–33].

Chirality of the superconductivity is also reflected in properties of vortex states. These properties were mainly studied in chiral p-wave superconductors. As for the pair potential, the opposite chiral component of the pair potential is induced around a vortex. The spatial structures of the induced components reflect the chirality, depending on whether the chirality is parallel ($L_z = +1$) or antiparallel ($L_z = -1$) to the vorticity ($w = +1$) [34–36]. Contributions of chirality also appear in behaviors of the LDOS in the vortex states [37–39]. In chiral p-wave superconductors, zero-energy bound states around a vortex have properties of Majorana states [40–42], accompanied with an odd-frequency Cooper-pair amplitude [43,44]. Related to these properties, only in the antiparallel case of $L_z = -1$, local NMR relaxation rate T_1^{-1} shows anomalous suppression at the vortex core region [45–49], and the zero-energy LDOS around a vortex are protected from the nonmagnetic impurity scattering effect in the Born limit [50,51]. Using the local T_1^{-1} or impurity effect on the vortex bound state, we can distinguish the chirality of p-wave superconductor, i.e., p_+-wave with $L_z = +1$ or p_--wave with $L_z = -1$.

The purpose of this work is to clarify characters of two chiral d-wave superconductors, $d_{1\pm}$ and $d_{2\pm}$, in comparison with the chiral $p_\pm$-wave superconductors, calculating spatial structure of the pair potential and the local electronic states in the vortex states. As for the pair potential, we study the contribution of the opposite chiral component induced around a

vortex. In the study of local electronic states, we also consider s-wave Cooper pair amplitude and the local scattering rate to understand the impurity effects on the LDOS. Our numerical calculations in the vortex lattice state are based on the Eilenberger theory [25,28,52–55], which is derived from Gor'kov theory in the superconducting state under the assumption $\Delta_0/E_F \ll 1$ for the superconducting gap Δ_0 and Fermi energy E_F. This condition is satisfied in many superconductors. The Eilenberger theory is suitable to treat inhomogeneous superconducting states, such as surface, interface, and vortex states. There, pair potential of superconductivity shows spatial variation in the length scale of the coherence length, which is longer than the atomic scale. By the calculations of self-consistent Eilenberger theory in the vortex lattice, we can obtain quantitative estimation in the whole range of temperature T and magnetic field B in the vortex states. There, we can appropriately evaluate the vortex core structure and the contributions from neighbor vortices.

To include contributions of nonmagnetic impurity scattering effects, we consider self-energy from the impurity scatterings. In addition to the Born limit [52,53], we study the unitary limit of the impurity scattering effects by the t-matrix approximation [56–63]. Therefore, our study covers the difference between the Born and unitary limits in the impurity scattering effects on the vortex states in chiral superconductors.

This paper is organized as follows. After this introduction, we explain our model and formulation in Sec. II. In Sec. III, we shortly see the impurity scattering effects in the uniform states in chiral superconductors. In Sec. IV, we study impurity scattering effects in the vortex states, calculating spatial structures of the pair potential, LDOS, s-wave Cooper pair amplitude, and local scattering rate. The last section is devoted to summary. In Appendix, impurity scattering effects on the vortex states are studied in an isotropic s-wave superconductor for a comparison with chiral superconductors.

II. FORMULATION BY SELF-CONSISTENT QUASICLASSICAL THEORY

For simplicity, we consider a two-dimensional cylindrical Fermi surface with a Fermi velocity $\boldsymbol{v}_F = v_{F0}(\cos\theta, \sin\theta, 0)$ at a Fermi wave number $\boldsymbol{k} = (k_F\cos\theta, k_F\sin\theta, k_z)$. The pair potential is given by

$$\Delta(\boldsymbol{r},\boldsymbol{k}) = \Delta_1(\boldsymbol{r})\varphi_{p,m}(\boldsymbol{k}) + \Delta_2(\boldsymbol{r})\varphi_{p,-m}(\boldsymbol{k}) \tag{1}$$

with the pairing function

$$\varphi_{p,\pm1}(\boldsymbol{k}) = (k_x \pm ik_y)/k_F = e^{\pm i\theta} \tag{2}$$

for chiral $p_\pm$-wave superconductors with $m = \pm1$. For chiral d-wave superconductors,

$$\Delta(\boldsymbol{r},\boldsymbol{k}) = \Delta_1(\boldsymbol{r})\varphi_{d,m}(\boldsymbol{k}) + \Delta_2(\boldsymbol{r})\varphi_{d,-m}(\boldsymbol{k}) \tag{3}$$

with

$$\varphi_{d,\pm1}(\boldsymbol{k}) = (k_x \pm ik_y)\sqrt{2}\sin k_z/k_F = e^{\pm i\theta}\sqrt{2}\sin k_z, \tag{4}$$

$$\varphi_{d,\pm2}(\boldsymbol{k}) = (k_x^2 - k_y^2 \pm i2k_xk_y)/k_F^2 = e^{\pm i2\theta}. \tag{5}$$

In this paper, the case of $m = \pm1$ ($m = \pm2$) is denoted as $d_{1\pm}$-wave ($d_{2\pm}$-wave) superconductors. $\boldsymbol{r}$ is the center-of-mass coordinate of the pair. $\Delta_1(\boldsymbol{r})$ is the main comportment of the pair potential. While $\Delta_2(\boldsymbol{r}) = 0$ in a uniform state, in the vortex state $\Delta_2(\boldsymbol{r})$ is induced by the spatial variation of the main component $\Delta_1(\boldsymbol{r})$ [34,35]. Magnetic fields $\boldsymbol{B}$ are applied along the z direction, and the vector potential is given by $\boldsymbol{A}(\boldsymbol{r}) = \frac{1}{2}\boldsymbol{B}\times\boldsymbol{r} + \boldsymbol{a}(\boldsymbol{r})$ in the symmetric gauge. The unit cell of the vortex lattice is set to be square lattice, which is realised in Sr_2RuO_4 [64–66]. $|\Delta(\boldsymbol{r})|$ and $\boldsymbol{a}(\boldsymbol{r})$ have periodicity of the vortex lattice. The structures of the pair potential and local electronic state in the vortex core are not significantly changed in the triangular vortex lattice case.

We calculate the spatial structure of vortices in the vortex lattice state by self-consistent Eilenberger theory [25,28,52,53], including self-energy from nonmagnetic s-wave impurity scatterings [54–63]. This method appropriately captures contributions of vortex core and inter-vortex interaction. In previous studies [55,58–60], the impurity scattering effects on the vortex states in the Born and the unitary limits were studied in nonchiral superconductors, such as s-, d-, and p_x-wave pairing. We extend the studies to the vortex states in chiral p and d-wave superconductors. In chiral p-wave superconductors, we compare the results in the unitary limit with those in the Born limit, which were reported in a previous study for a single vortex [51].

In Eilenberger theory, to obtain quasiclassical Green's functions

$$f(i\omega_n,\boldsymbol{k},\boldsymbol{r}) = \frac{2a}{1+ab}, \quad f^\dagger(i\omega_n,\boldsymbol{k},\boldsymbol{r}) = \frac{2b}{1+ab},$$
$$g(i\omega_n,\boldsymbol{k},\boldsymbol{r}) = \frac{1-ab}{1+ab}, \tag{6}$$

we calculate $a(i\omega_n,\boldsymbol{k},\boldsymbol{r})$ and $b(i\omega_n,\boldsymbol{k},\boldsymbol{r})$ by numerical integration of Riccati equations [26,67,68]

$$\begin{aligned}\boldsymbol{v}\cdot\nabla a &= \Delta + F - \left(\Delta^* + F^\dagger\right)a^2 \\ &\quad - (\omega_n + G + i\boldsymbol{v}\cdot\boldsymbol{A})a, \\ -\boldsymbol{v}\cdot\nabla b &= \Delta^* + F^\dagger - (\Delta + F)b^2 \\ &\quad - (\omega_n + G + i\boldsymbol{v}\cdot\boldsymbol{A})b\end{aligned} \tag{7}$$

along the trajectory parallel to the vector $\boldsymbol{v} = \boldsymbol{v}_F/v_{F0}$. In our calculations, length, temperature, and magnetic field are, respectively, measured in unit of ξ_0, T_c, and B_0. Here, $\xi_0 = \hbar v_{F0}/2\pi k_B T_c$ and $B_0 = \phi_0/2\pi\xi_0^2$ with the flux quantum ϕ_0. T_c is superconducting transition temperature in the clean limit at $B = 0$. The energy E, pair potential Δ and Matsubara frequency ω_n are in unit of $\pi k_B T_c$. Within the t-matrix approximation [54–58,61–63], self-energies $G(i\omega_n,\boldsymbol{r})$, $F(i\omega_n,\boldsymbol{r})$, and $F^\dagger(i\omega_n,\boldsymbol{r})$ in Eq. (7) are given by

$$G = \frac{1}{\tau}\langle g\rangle_{\boldsymbol{k}}, \; F = \frac{1}{\tau}\langle f\rangle_{\boldsymbol{k}}, \; F^\dagger = \frac{1}{\tau}\langle f^\dagger\rangle_{\boldsymbol{k}}, \tag{8}$$

with local scattering rate $1/\tau(\boldsymbol{r})$ in superconductors,

$$\frac{1}{\tau} = \frac{1/\tau_0}{\cos^2\delta_0 + (\langle g\rangle_{\boldsymbol{k}}^2 + \langle f\rangle_{\boldsymbol{k}}\langle f^\dagger\rangle_{\boldsymbol{k}})\sin^2\delta_0}, \tag{9}$$

and $\delta_0 = \tan^{-1}(\pi N_0 u_0)$ with impurity strength u_0. $\langle\cdots\rangle_{\boldsymbol{k}}$ indicates the Fermi surface average. N_0 is the density of states (DOS) at the Fermi energy in the normal state. In the Born limit of weak impurity scattering potential, $\delta_0 \to 0$. In the

unitary limit of strong scattering potential, $\delta_0 \to \pi/2$. The scattering time τ_0 in the normal state is given by

$$\frac{1}{\tau_0} = \frac{n_s N_0 u_0^2}{1 + \pi^2 N_0^2 u_0^2}, \tag{10}$$

where n_s is the number density of impurities. τ_0 is in unit of $\hbar/2\pi k_B T_c$ [55]. The mean-free-path l is given by $l/\xi_0 = v_{F0}\tau_0/(\hbar v_{F0}/2\pi k_B T_c) = \tau_0/(\hbar/2\pi k_B T_c) = \tau_0$ in our unit. Within the t-matrix approximation of the impurity scatterings, we can study continuous crossover from clean superconductors to dirty ones, including suppression of anisotropic superconductivity by nonmagnetic impurity scatterings. We note that the t-matrix approximation [54–63] following Abrikosov-Gor'kov theory [69] considers the situation where the average on the random position of the independent impurity centers is possible even when we study phenomena in the scale of the superconducting coherence length, and regards $\Delta(\boldsymbol{r})$ as very nearly independent of impurity configuration [69–72]. This may cause discussions on the application of this formalism to the clean case where l is larger than the vortex core radius in the order of ξ_0, while it depends on parameter choices of n_s, N_0, and u_0 in Eq. (10).

As self-consistent conditions, the pair potentials $\Delta_1(\boldsymbol{r}) = \Delta_{l,m}(\boldsymbol{r})$ and $\Delta_2(\boldsymbol{r}) = \Delta_{l,-m}(\boldsymbol{r})$ in Eqs. (1) or (3) are calculated by the gap equation

$$\Delta_{l,m}(\boldsymbol{r}) = g_0 N_0 T \sum_{0<\omega_n\leqslant\omega_{\rm cut}} \langle \varphi^*_{l,m}(f + f^{\dagger *})\rangle_{\boldsymbol{k}} \tag{11}$$

for $l = p$, d, and $m = \pm 1$, ± 2, with $(g_0 N_0)^{-1} = \ln T + 2T\sum_{0<\omega_n\leqslant\omega_{\rm cut}} \omega_n^{-1}$. We use $\omega_{\rm cut} = 20 k_B T_c$. The vector potential for the internal magnetic field is self-consistently determined by

$$\nabla \times (\nabla \times \boldsymbol{A}) = -\frac{2T}{\kappa^2} \sum_{0<\omega_n} \langle \boldsymbol{v}\, {\rm Im}\{g\}\rangle_{\boldsymbol{k}}. \tag{12}$$

We set the Ginzburg-Landau parameter κ to be large as $\kappa = 30$ assuming typical type-II superconductors.

First, we self-consistently solve Eqs. (6)–(12) at $T = 0.5T_c$ for some $1/\tau_0$ in the Born and the unitary limits [59,60]. Next, in the calculations of local electronic states, using $\Delta(\boldsymbol{r})$ and $\boldsymbol{A}(\boldsymbol{r})$ obtained in the above calculation of ω_n, we self-consistently solve Eqs. (6)–(9) with $i\omega_n \to E + i\eta$ to obtain quasiclassical Green's functions and the selfenergies as a function of real energy E. η is an infinitesimal constant. The LDOS $N(E, \boldsymbol{r})$ and the s-wave Cooper pair amplitude $f_s(E, \boldsymbol{r})$ are, respectively, obtained by

$$N(E, \boldsymbol{r})/N_0 = \langle {\rm Re}\{g(i\omega_n \to E + i\eta, \boldsymbol{k}, \boldsymbol{r})\}\rangle_{\boldsymbol{k}}, \tag{13}$$

$$f_s(E, \boldsymbol{r}) = \langle f(i\omega_n \to E + i\eta, \boldsymbol{k}, \boldsymbol{r})\rangle_{\boldsymbol{k}}. \tag{14}$$

III. IMPURITY EFFECTS IN UNIFORM STATES

Before studying the vortex states, we evaluate suppression of superconductivity by the nonmagnetic impurity scattering in uniform states at a zero magnetic field without vortices. In the uniform state, Δ_1 is a constant and $\Delta_2 = 0$. Figure 1 shows $1/\tau_0$ dependence of uniform $|\Delta_1|$ at $T/T_c = 0.5$ for each pairing symmetry.

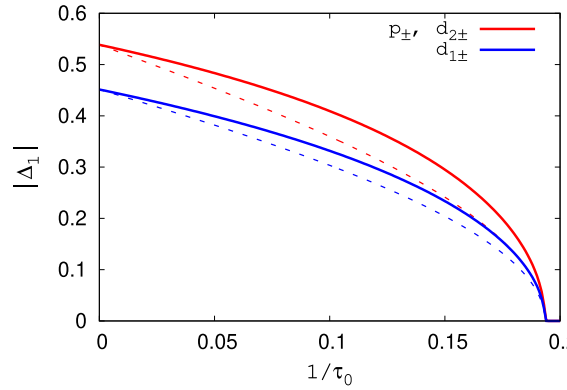

FIG. 1. Amplitude of the pair potential Δ_1 as a function of $1/\tau_0$ in uniform states at a zero field in chiral $p_\pm$, $d_{1\pm}$, and $d_{2\pm}$-wave superconductors. Solid (dashed) lines are for the Born (unitary) limit. $|\Delta_1|$s of $p_\pm$ and $d_{2\pm}$-wave superconductors are on the same line. $T/T_c = 0.5$.

In Fig. 1, we see that chiral d-wave superconductors are easily suppressed by the nonmagnetic impurity scattering effects, as in the chiral p-wave superconductors. The $d_{2\pm}$-wave superconductors have the same $1/\tau_0$ dependence of $|\Delta_1|$ as that in the chiral $p_\pm$-wave superconductors. These pairings have isotropic gap amplitude as $|\varphi_{d,\pm 2}| = |\varphi_{p,\pm 1}| = 1$. Compared to these pairing symmetries, the $d_{1\pm}$-wave superconductors have smaller $|\Delta_1|$ due to the horizontal line node of $|\varphi_{d,\pm 1}| = \sqrt{2}|\sin k_z|$. In each pairing symmetry, $|\Delta_1|$ in the unitary limit is smaller than that in the Born limit at finite $1/\tau_0$, since effective $1/\tau$ in Eq. (9) is enhanced in the unitary limit as discussed later.

IV. IMPURITY EFFECTS IN VORTEX STATES

A. Spatial structure of pair potential

First we study the spatial structure of the pair potential in chiral superconductors in the presence of impurity scattering effects at $T/T_c = 0.5$ and $B/B_0 = 0.01$. Figure 2 presents vortex states in chiral p_+ and p_--wave superconductors comparatively. Figure 3 is for chiral d_{1+} and d_{1-}-wave superconductors. Comparing the pair potentials in Figs. 2(a) and 2(b) for $p_\pm$-wave and Figs. 3(a) and 3(b) for $d_{1\pm}$-wave, the spatial structure of the pair potential is almost identical in $p_\pm$ and $d_{1\pm}$-wave superconductors, while the amplitude is slightly smaller in $d_{1\pm}$-wave.

We study the detailed spatial structure of the pair potentials in these figures. Main component $|\Delta_1(\boldsymbol{r})|$ in Fig. 2(a) shows conventional vortex structure, where $|\Delta_1(\boldsymbol{r})|$ is suppressed at the vortex core near $r = 0$, and recovered towards uniform value far from the vortex. With increasing $1/\tau_0$, the amplitude of the pair potential is decreased, reflecting the suppression of the superconductivity by the impurity scattering effects as explained in Fig. 1. The vortex core radius becomes longer for larger $1/\tau_0$. There, $|\Delta_1(\boldsymbol{r})|$ is smaller in the unitary limit than in the Born limit. These behaviors are almost the same between the p_+ and p_--wave superconductors, as is seen in Fig. 2(a).

The induced opposite chiral component $|\Delta_2(\boldsymbol{r})|$ is presented in Fig. 2(b). There are larger differences in the

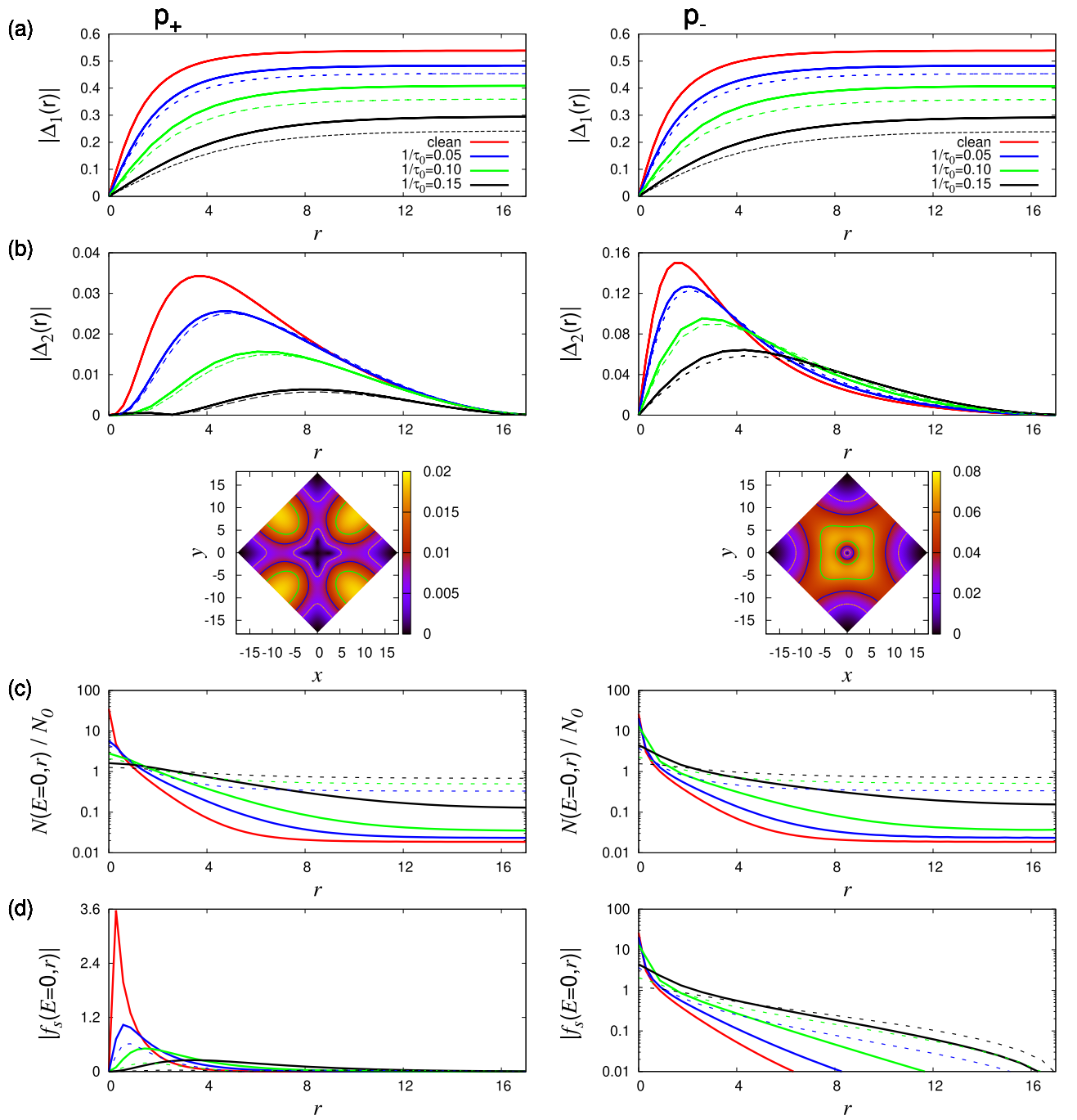

FIG. 2. Vortex states in chiral p_+-wave (left) and p_--wave (right) superconductors for $1/\tau_0 = 0$, 0.05, 0.10, and 0.15 in the Born and the unitary limits. $T/T_c = 0.5$. $B/B_0 = 0.01$. (a) Main component $|\Delta_1(\boldsymbol{r})|$ of the pair potential, (b) induced opposite chiral component $|\Delta_2(\boldsymbol{r})|$, (c) zero energy LDOS $N(E = 0, \boldsymbol{r})/N_0$, and (d) s-wave Cooper pair amplitude $|f_s(E = 0, \boldsymbol{r})|$, as a function of radius r along x axis of next nearest neighbor (NNN) vortex direction. The units of length r are ξ_0. Solid (dashed) lines are for the Born (unitary) limit. In (c) and the right panel of (d), the vertical axis is a logarithmic scale. In (b), we also show density plot of $|\Delta_2(\boldsymbol{r})|$ within a unit cell of the vortex lattice in (x, y) plane for $1/\tau_0 = 0.15$ in the Born limit. There, the vortex is located at the center of the unit cell and cuts of the r dependence in (a)–(d) are along the x axis from the vortex center.

magnitude and the structure of $|\Delta_2(\boldsymbol{r})|$ between p_+ and p_--wave superconductors, as reported in previous studies in the clean limit [34,35]. The amplitude $|\Delta_2(\boldsymbol{r})|$ is much smaller in the p_+-wave superconductors. In the clean limit, the maximum is $|\Delta_2(\boldsymbol{r})| \sim 0.15$ (0.034) in the p_--wave (p_+-wave) superconductor. In the presence of impurity effects, with increasing $1/\tau_0$, $|\Delta_2(\boldsymbol{r})|$ becomes smaller, corresponding to the decrease of the main component $|\Delta_1(\boldsymbol{r})|$ in Fig. 2(a). The peak position is shifted to larger r, reflecting increase of the vortex core radius. These impurity effects on $|\Delta_2(\boldsymbol{r})|$ are similar between the Born and the unitary limits, while $|\Delta_2(\boldsymbol{r})|$ is slightly smaller in the unitary limit. The differences between both limits are smaller in $|\Delta_2(\boldsymbol{r})|$ than that of $|\Delta_1(\boldsymbol{r})|$.

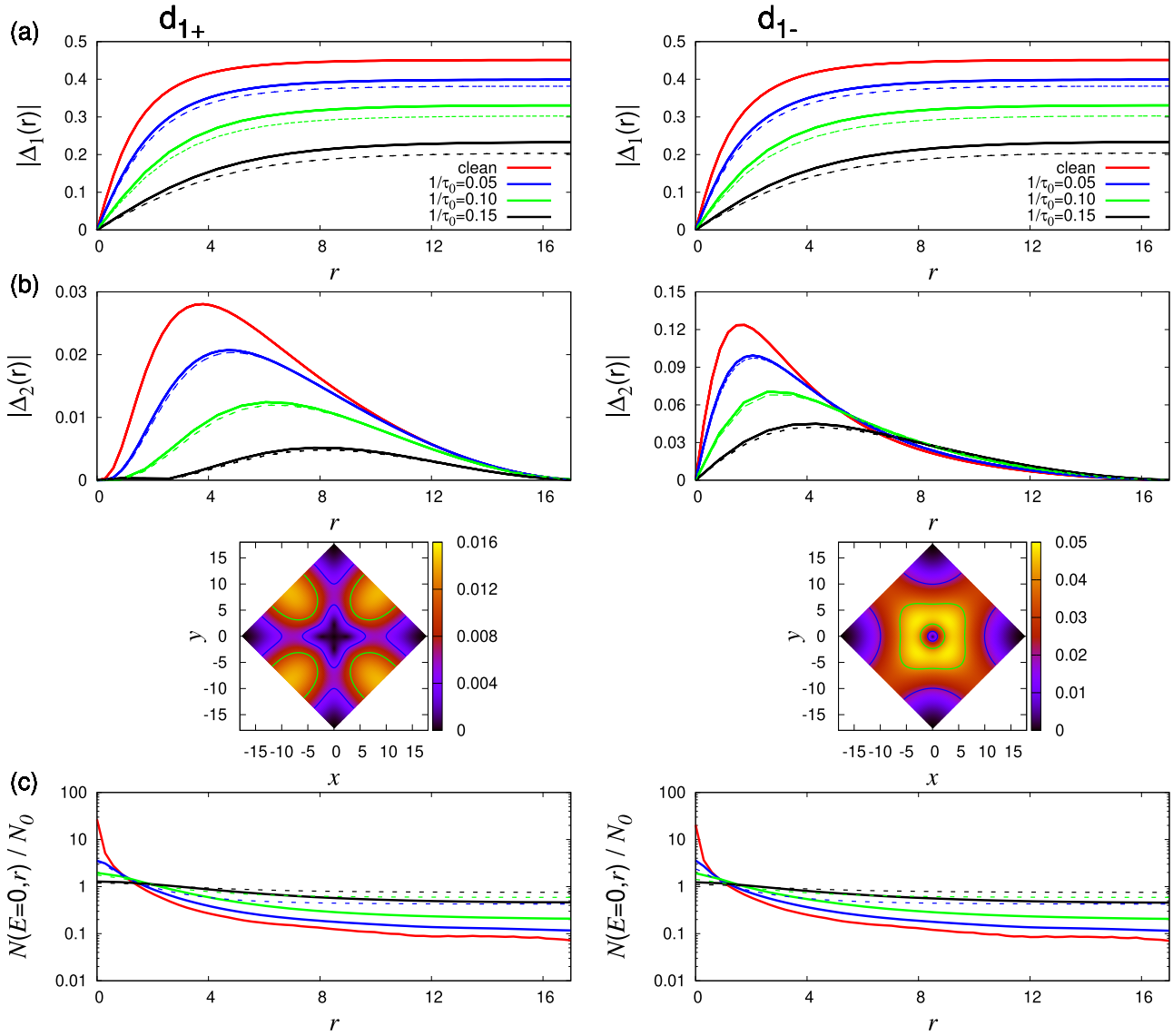

FIG. 3. The same as Figs. 2(a)–2(c), but for d_{1+}-wave (left panels) and d_{1-}-wave (right panels) superconductors. The s-wave Cooper pair amplitude is zero in $d_{1\pm}$-wave superconductors.

Comparing Figs. 2(a), 2(b) and 3(a), 3(b) we see that a d_{1+} (d_{1-}) wave superconductor has similar spatial structure of the pair potential to that in the p_+ (p_-) wave superconductor, as both pairing symmetry has the angular momentum $L_z = 1$ (-1).

The spatial structure of $\Delta_2(\boldsymbol{r})$ is related to the relation that $m + w$ keeps constant around a vortex [48,51], as presented in Table I. There, w is a winding number around a vortex for $\Delta_{l,m}(\boldsymbol{k})$ and the Cooper pair component $f_{l,m}(E = 0, \boldsymbol{r})$, defined as $f_{l,m}(E, \boldsymbol{r}) = \langle \varphi^*_{l,m} f(i\omega_n \to E + i\eta, \boldsymbol{k}, \boldsymbol{r}) \rangle_{\boldsymbol{k}}$, with chirality m. In each superconductor, the main component $\Delta_1(\boldsymbol{r})$ has a winding $w = +1$ at the vortex center. In p_- and d_{1-}-wave superconductors, since $\Delta_2(\boldsymbol{r})$ with $m = 1$ has winding $w = -1$ around a vortex center, $|\Delta_2(\boldsymbol{r})|$ is linearly recovered from the vortex center [34,35], as seen in right panels of Figs. 2(b) and 3(b). To compensate the winding -1 at the vortex center, additional winding $+2$ appears at each corner (i.e., midpoint $r = 17.7\xi_0$ between NNN vortices) of unit cell of the vortex lattice so that total winding keeps $+1$ within a

TABLE I. Winding number w around a vortex center in Cooper pair components $f_{l,m}(E = 0, \boldsymbol{r})$ and $\Delta_{l,m}(\boldsymbol{r})$ with chirality m when main components of superconductivity are, respectively, $d_{2\pm}$, $d_{1\pm}$, $p_\pm$, and s-wave pairing symmetries. $w = +1$ by solid font is for the main component with vortex winding $+1$. w with underline indicates the winding number in the induced opposite chiral component of the pair potential. In rows for each pairing symmetry, $m + w$ keeps a constant value.

Main	Chirality of Cooper pair amplitude				
super-conductivity	$m = 2$ (d_{2+})	$m = 1$ (d_{1+}, p_+)	$m = 0$ (s)	$m = -1$ (d_{1-}, p_-)	$m = -2$ (d_{2-})
d_{2+}	$w = +\mathbf{1}$	$+2$	$+3$	$+4$	$\underline{+5}$
d_{1+}, p_+	$w = 0$	$+\mathbf{1}$	$+2$	$\underline{+3}$	$+4$
s	$w = -1$	0	$+\mathbf{1}$	$+2$	$+3$
d_{1-}, p_-	$w = -2$	$\underline{-1}$	0	$+\mathbf{1}$	$+2$
d_{2-}	$w = \underline{-3}$	-2	-1	0	$+\mathbf{1}$

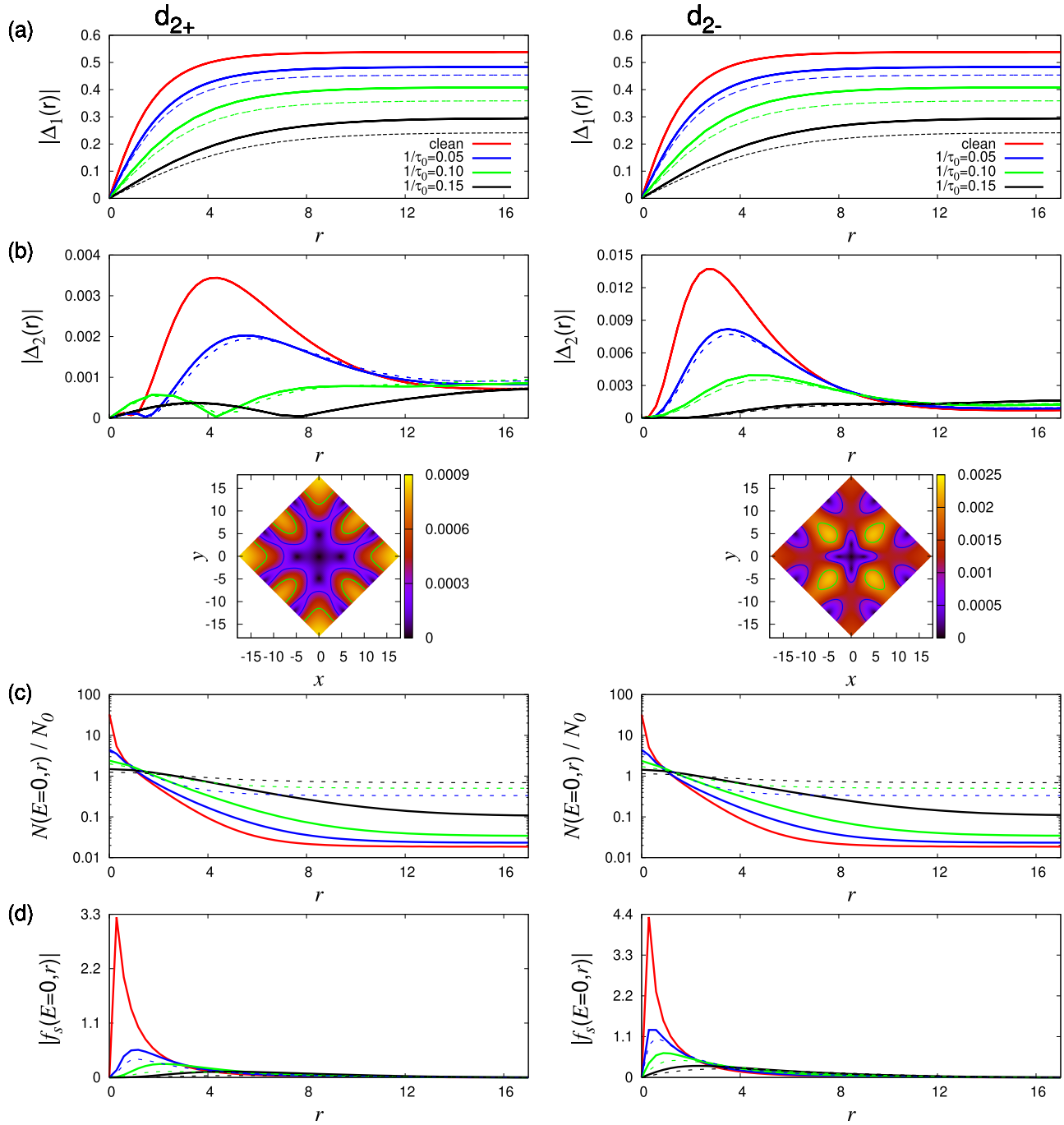

FIG. 4. The same as Fig. 2, but for d_{2+}-wave (left) and d_{2-}-wave (right) superconductors.

unit cell [35]. In the p_+ and d_{1+}-wave superconductors, $\Delta_2(\boldsymbol{r})$ with $m = -1$ has winding $w = +3$ around a vortex center, where $|\Delta_2(\boldsymbol{r})| \propto r^3$ for smaller $1/\tau_0$ [34,35]. When the superconductivity is suppressed by the impurity scattering effects for larger $1/\tau_0$, the winding $+3$ at $r = 0$ splits to four winding $+1$ at finite r and winding -1 at $r = 0$. This split occurs also in the high field case in the clean limit [35]. Therefore, for larger $1/\tau_0$ in left panels of Figs. 2(b) and 3(b), $|\Delta_2(\boldsymbol{r})|$ has zero at the winding $+1$ points at finite r along x and y axes. As presented in lower panels of Fig. 2(b), $|\Delta_2(\mathbf{r})|$ has fourfold symmetric spatial distribution around a vortex, while $|\Delta_1(\mathbf{r})|$ shows almost circular symmetric vortex core shape.

Next, we study the pair potential in d_{2+} and d_{2-}-wave superconductors shown in Fig. 4. The main component $|\Delta_1(\boldsymbol{r})|$ shows conventional behaviors of impurity effects similar to those in $p_\pm$ and $d_{1\pm}$-wave superconductors. However, the induced opposite chiral component $\Delta_2(\boldsymbol{r})$ shows different spatial structure. In the d_{2+}-wave superconductor, as shown in Table I, $\Delta_2(\boldsymbol{r})$ has winding $+5$ around the vortex center. In the density plot of $|\Delta_2(\boldsymbol{r})|$ for $1/\tau_0 = 0.05$ in the left panel of Fig. 4(b), the winding $+5$ at the vortex center splits to five singular points of winding $+1$ at $r = 0$ and at finite r on x and y axes. To compensate the winding $+5$ around the vortex center, additional eight singular points of winding -1

are located on the boundary lines of a unit cell. Due to the existence of many singular winding points, amplitude $|\Delta_2(\boldsymbol{r})|$ is very small, since it can not enoughly recover from the singular points. With increasing $1/\tau_0$, $|\Delta_2(\boldsymbol{r})|$ becomes further smaller, and singular points with winding $+1$ at finite r shift to larger r near the vortex center, as shown in left panels of Fig. 4(b).

On the other hand, from the relation in Table I, $\Delta_2(\boldsymbol{r})$ in the d_{2-}-wave superconductor has winding -3 around the vortex center. Thus $|\Delta_2(\mathbf{r})| \propto r^3$ for smaller $1/\tau_0$. As seen in the density plot in right panel of Fig. 4(b), to compensate winding -3 around the vortex center, additional eight singular points with winding $+1$ appear on the boundary lines of the unit cell. Therefore $|\Delta_2(\boldsymbol{r})|$ is smaller than those of p_+ and d_{1+}-wave superconductors. With increasing $1/\tau_0$, $|\Delta_2(\boldsymbol{r})|$ becomes further smaller as is seen in the right panel of Fig. 4(b). There, at larger $1/\tau_0$, $|\Delta_2(\boldsymbol{r})|$ has zero also at finite r, as the winding -3 at the vortex center splits to a winding $+1$ at $r = 0$ and four singular points of winding -1 at finite r. Also in $d_{2\pm}$-wave superconductors, the difference between the Born and the unitary limits is very small in $|\Delta_2(\boldsymbol{r})|$, compared with $|\Delta_1(\boldsymbol{r})|$.

It is known that some of exotic properties in chiral superconductors come from the spatial structure of the opposite chiral component $\Delta_2(\boldsymbol{r})$ [34–36,65,66]. They contribute to the free energy difference between the cases when the chirality is parallel ($L_z > 0$) or antiparallel ($L_z < 0$) to the vortex winding, so that one of the chiral directions becomes stable in the vortex states under magnetic fields. The chiral direction dependence of $\Delta_2(\boldsymbol{r})$ induces the chirality dependence of the spatial structure of the supercurrents, internal fields, and the LDOS. The vortex lattice becomes square lattice by the contribution of $\Delta_2(\boldsymbol{r})$. About these phenomena, we can expect similar behaviors in chiral $d_{1\pm}$-wave superconductors to those in chiral $p_\pm$-wave superconductors, respectively, because $\Delta_2(\boldsymbol{r})$ shows similar structure in Figs. 2(b) and 3(b). However, in chiral $d_{2\pm}$-wave superconductors, since $\Delta_2(\boldsymbol{r})$ in Fig. 4(b) has different spatial structure and small amplitude, the chirality dependent behaviors by $\Delta_2(\boldsymbol{r})$ may be different and weak, compared with chiral $p_\pm$-wave superconductors. The differences between d_{2+} and d_{2-}-wave superconductors are small, and the detection may be more difficult.

B. Local electronic states at the vortex core

In zero-energy LDOS $N(E = 0, \boldsymbol{r})$ in Figs. 2(c), 3(c), and 4(c), we see a sharp peak at the vortex center $r = 0$, as the bound state is localized in the vortex core. In the clean limit, $N(E = 0, \boldsymbol{r})$ is well confined around a vortex core in $p_\pm$- and $d_{2\pm}$-wave superconductors with full gap. Compared with them, $N(E = 0, \boldsymbol{r})$ extends broader from the vortex core in $d_{1\pm}$-wave superconductors due to the horizontal line node. With increasing impurity scattering rate $1/\tau_0$, the peak height becomes lower and the width broader.

Outside of vortex, $N(E = 0, \boldsymbol{r})$ is reduced to the DOS in the uniform state of bulk. In the Born limit, it does not appear at small $1/\tau_0$, and slowly increases at larger $1/\tau_0$. On the other hand, in the unitary limit, the zero energy DOS easily appears by small $1/\tau_0$ even outside of vortex. There, bulk impurity scattering states and the vortex bound states are mixed in $N(E = 0, \boldsymbol{r})$ in the vortex core.

To see the impurity scattering effects on the peak height $N(E = 0, r = 0)$ at the vortex center in Fig. 2(c) in chiral $p_\pm$-wave superconductors, we plot $1/\tau_0$ dependence of $N(E = 0, r = 0)$ in Fig. 5(a). As was reported in Ref. [51] for a single vortex, in the Born limit the peak height in the p_--wave superconductor slowly decreases as a function of $1/\tau_0$, but it rapidly decreases in the p_+-wave superconductor. On the other hand, in the unitary limit our results show the similar rapid decrease of the peak height both in the p_+-wave and p_--wave superconductors. Therefore the anomalous $1/\tau_0$ dependence of $N(E = 0, r = 0)$ in the Born limit vanishes in the unitary limit.

In chiral $d_{1\pm}$-wave superconductors in Fig. 5(b) corresponding to Fig. 3(c), the peak height in the d_{1-}-wave superconductor rapidly decreases even in the Born limit. The peak heights in d_{1+}-wave and d_{1-}-wave superconductors similarly decrease as a function of $1/\tau_0$ both in the Born and the unitary limits. We note that the peak height is larger in the d_{1+}-wave superconductors for cleaner case of small $1/\tau_0$. This behavior is similar to that in the $p_\pm$-wave superconductor. There, compared to the p_--wave superconductor, the peak is higher in the p_+-wave superconductor at $1/\tau_0 = 0$ in Fig. 5(a).

Also in chiral $d_{2\pm}$-wave superconductors in Fig. 5(c) corresponding to Fig. 4(c), the peak heights in d_{2+} and d_{2-}-wave superconductors show similar rapid decreases as a function of $1/\tau_0$ both in the Born and the unitary limits. The differences between d_{2+} and d_{2-}-wave superconductors and between the Born and the unitary limits are very small, compared to the $d_{1\pm}$-wave superconductors.

C. *s*-wave Cooper pair amplitude

As is seen in the previous subsection, the zero-energy vortex bound states are strong against the nonmagnetic impurity scattering only in the p_--wave superconductor in the Born limit. The reason for this property was explained in relation to the odd frequency s-wave Cooper pair amplitude in Ref. [51]. There the s-wave Cooper pair amplitude, appearing at the vortex core, is strong to the nonmagnetic impurity scattering due to the Anderson theorem [69,73].

In chiral p-wave superconductors, zero energy bound state at the vortex has a property of Majorana state [40–42]. Related to the Majorana property, zero-energy state has the relation [44,49].

$$N(E = 0, \boldsymbol{r})/N_0 = |f_s(E = 0, \boldsymbol{r})|. \tag{15}$$

Therefore, in our study about the impurity scattering effects, we estimate the zero-energy s-wave Cooper pair amplitude $|f_s(E = 0, \boldsymbol{r})|$ in comparison with $N(E = 0, \boldsymbol{r})/N_0$. In $p_\pm$-wave superconductors, the s-wave Cooper pair amplitude is in the odd-frequency symmetry [43,44].

Spatial structures of $|f_s(E = 0, \boldsymbol{r})|$ in $p_\pm$-, $d_{1\pm}$- and $d_{2\pm}$-wave superconductors are, respectively, presented in Figs. 2(d), 3(d), and 4(d). As shown in a right panel of Fig. 2(d), $|f_s(E = 0, \boldsymbol{r})|$ has a sharp peak at the vortex center in a chiral p_--wave superconductor. With increasing $1/\tau_0$, the peak height and the width becomes lower and broader, respectively. Comparing it with the right panel of Fig. 2(c),

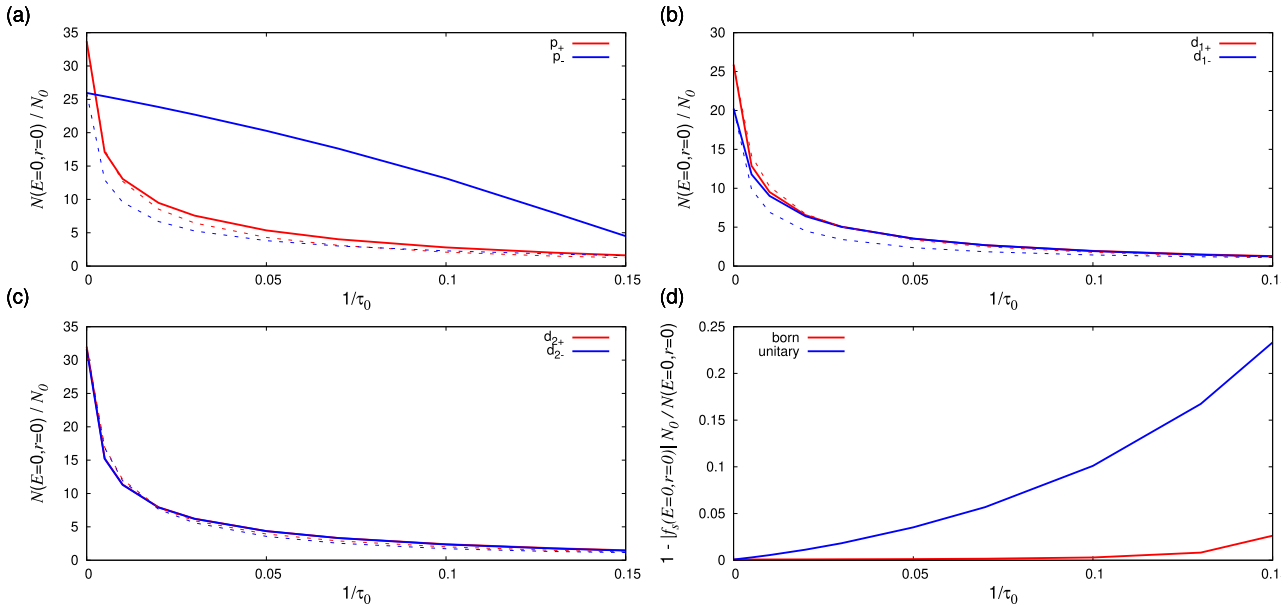

FIG. 5. Peak height of zero-energy LDOS $N(E=0, r=0)/N_0$ at the vortex center as a function of $1/\tau_0$ in (a) $p_\pm$-wave, (b) $d_{1\pm}$-wave, and (c) $d_{2\pm}$-wave superconductors. (d) The difference of zero-energy LDOS and the odd frequency s-wave Cooper pair amplitude at the vortex center in the p_--wave superconductor. We plot $1 - |f_s(E=0, r=0)|N_0/N(E=0, r=0)$. In (a)–(c), solid and dashed lines are, respectively, for the Born and the unitary limits.

we see that $|f_s(E=0, \boldsymbol{r})|$ shows similar behaviors to $N(E=0, \boldsymbol{r})/N_0$ around a vortex. We plot them in Fig. 6 to confirm that the relation in Eq. (15) is well satisfied even for finite $1/\tau_0$ at the vortex core region in the Born limit. The relation breaks outside of vortex core. Far from the vortex, $|f_s(E=0, \boldsymbol{r})| \to 0$, while $N(E=0, \boldsymbol{r})/N_0$ is reduced to a small finite value.

On the other hand, in the unitary limit, we see the deviation from the relation of Eq. (15) even in the vortex core region for larger $1/\tau_0$. Outside of vortex core $N(E=0, \boldsymbol{r})/N_0$ and $|f_s(E=0, \boldsymbol{r})|$ are larger compared with the Born limit, and their contrast between the vortex core and the outside is smeared. This enhancement of $N(E=0, \boldsymbol{r})/N_0$ outside of the vortex comes from the zero-energy impurity scattering states of bulk, which appear even in uniform states in the unitary limit. Since the excess bulk components penetrate inside of vortex core, $N(E=0, \boldsymbol{r})/N_0$ is slightly larger than $|f_s(E=0, \boldsymbol{r})|$ at the vortex core.

To estimate the relation of Eq. (15) at the vortex center, we plot deviation $(N(E=0, r=0)/N_0 - |f_s(E=0, r=0)|)/(N(E=0, r=0)/N_0) = 1 - |f_s(E=0, r=0)|N_0/N(E=0, r=0)$ as a function of $1/\tau_0$ in Fig. 5(d). There, we see the deviation increases as a function of $1/\tau_0$ in the unitary limit. In the Born limit, we see that the deviation is almost zero at $1/\tau_0 < 0.1$, satisfying Eq. (15). This difference between the Born and the unitary limits may be related to the fact that the zero-energy vortex core state in the p_--wave superconductor is strong to the impurity scattering only in the Born limit in Fig. 5(a), following the scenario suggested in Ref. [51].

In Table I, the column of $m=0$ indicates the winding number of the s-wave Cooper pair component $f_s(E=0, \boldsymbol{r})$ around a vortex center. Only in the p_--wave superconductor, $|f_s(E=0, \boldsymbol{r})|$ is finite at the vortex center, since the winding number $w=0$. As for other chiral superconductors, winding numbers abound a vortex are $+3$, $+2$, and -1 in

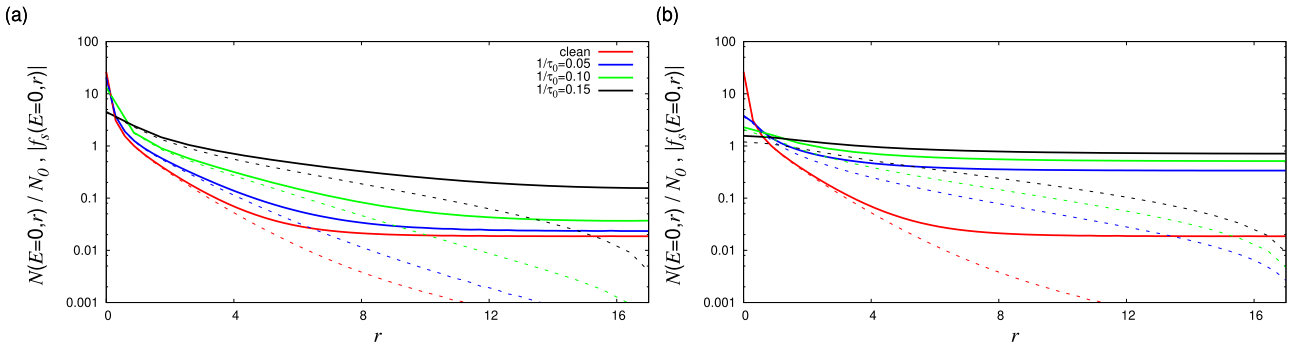

FIG. 6. Comparison of $N(E=0, \boldsymbol{r})/N_0$ (solid lines) and $|f_s(E=0, \boldsymbol{r})|$ (dashed lines) as a function of radius r along the NNN vortex direction for $1/\tau_0 = 0$, 0.05, 0.10, and 0.15 in (a) the Born and (b) unitary limits in a chiral p_--wave superconductor.

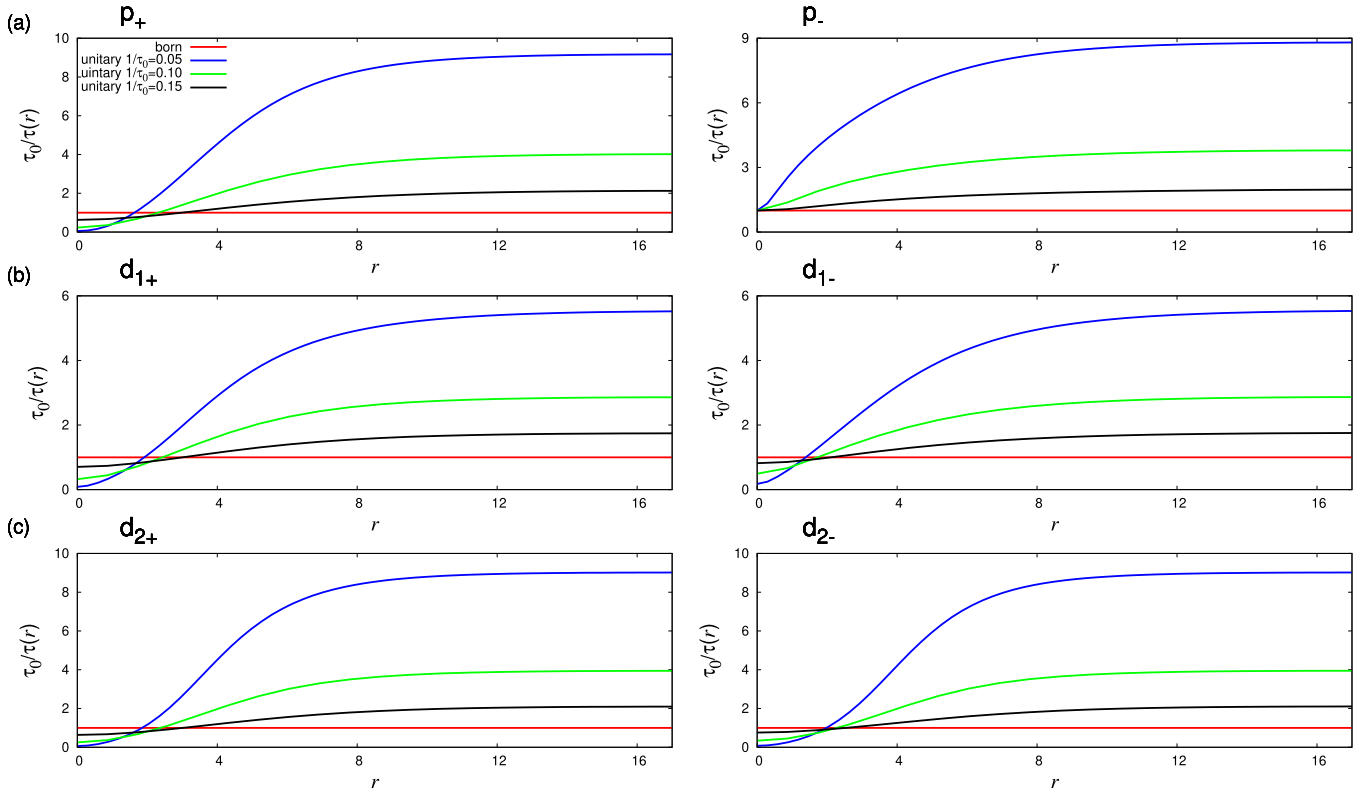

FIG. 7. Local scattering rate $\tau_0/\tau(\boldsymbol{r})$ from Eq. (9) for $E = 0$ in the unitary limit as a function of radius r in (a) $p_\pm$-wave, (b) $d_{1\pm}$-wave, and (c) $d_{2\pm}$-wave superconductors. $1/\tau_0 = 0.05$, 0.10, and 0.15. Left (right) panels are, respectively, for p_+, d_{1+}, and d_{2+} (p_-, d_{1-}, and d_{2-}). In the Born limit $\tau_0/\tau(\boldsymbol{r}) = 1$.

d_{2+}, p_+, and d_{2-}-wave superconductors, respectively. Therefore, in these superconductors, s-wave Cooper pair amplitude vanishes at the vortex center, as shown in Figs. 2(d) and 4(d). In $d_{1\pm}$-wave superconductors, since $f(E = 0, \boldsymbol{k}, \boldsymbol{r})$ is an odd function under the transformation $k_z \to -k_z$, the s-wave Cooper pair component $\langle f(E = 0, \boldsymbol{k}, \boldsymbol{r})\rangle_{\boldsymbol{k}} = 0$ after the Fermi surface average. Therefore, in chiral superconductors other than the p_--wave, the relation of Eq. (15) is not satisfied, since $f_s(E = 0, \boldsymbol{r})$ vanishes at the vortex center. This may be a reason for that the zero-energy vortex bound state is not strong against the impurity scattering in Fig. 5, following the scenario suggested in Ref. [51].

In the clean limit of p_+- and $d_{2\pm}$-wave superconductors, $|f_s(E = 0, \boldsymbol{r})|$ increases with approaching vortex from the outside, and after a peak it rapidly decreases to zero at $r \to 0$. With increasing the scattering rate $1/\tau_0$, the peak position shifts to farther from the vortex center, and the peak height becomes lower. In these superconductors, $|f_s(E = 0, \boldsymbol{r})|$ becomes smaller in the unitary limit, compared with the Born limit.

D. Local scattering rate in the unitary limit

While scattering rate $1/\tau(\boldsymbol{r})$ in Eq. (9) is a constant as $\tau_0/\tau(\boldsymbol{r}) = 1$ in the Born limit, $\tau_0/\tau(\boldsymbol{r}) = (\langle g\rangle_{\boldsymbol{k}}^2 + \langle f\rangle_{\boldsymbol{k}}\langle f^\dagger\rangle_{\boldsymbol{k}})^{-1}$ in the unitary limit has spatial variation due to the $\boldsymbol{r}$ dependence of $\langle g\rangle_{\boldsymbol{k}}$ and $\langle f\rangle_{\boldsymbol{k}}$. To discuss the differences between the Born and the unitary limits, we present the spatial structure of the local scattering rate $\tau_0/\tau(\boldsymbol{r})$ of the unitary limit for $E = 0$ in Fig. 7.

In all chiral superconductors in Fig. 7, outside of the vortex core, $1/\tau(\boldsymbol{r})$ is enhanced than $1/\tau_0$, being effectively dirtier in the unitary limit than in the Born limit. This is because $\langle g\rangle_{\boldsymbol{k}}^2 + \langle f\rangle_{\boldsymbol{k}}\langle f^\dagger\rangle_{\boldsymbol{k}} < 1$, reflecting $\langle f\rangle_{\boldsymbol{k}} = \langle f^\dagger\rangle_{\boldsymbol{k}} = 0$ in the uniform state where $f \propto \varphi_{l,m}(\boldsymbol{k})$ and $f^\dagger \propto \varphi_{l,m}^*(\boldsymbol{k})$. Therefore $\tau_0/\tau(\boldsymbol{r}) = \langle g\rangle_{\boldsymbol{k}}^{-2} = (N(E = 0, \boldsymbol{r})/N_0)^{-2} > 1$, since $N(E = 0, \boldsymbol{r}) < N_0$ in uniform superconducting states. With increasing $1/\tau_0$ toward dirtier superconductors, since $N(E = 0, \boldsymbol{r})/N_0$ of the uniform states becomes larger due to the impurity state in the unitary limit, $\tau_0/\tau(\boldsymbol{r})$ decreases and reduces to 1. Compared with the $d_{1\pm}$-wave superconductors with a horizontal line node, $\tau_0/\tau(\boldsymbol{r})$ is larger in $p_\pm$ and $d_{2\pm}$-wave superconductors with full gap.

Next, we study $\tau_0/\tau(\boldsymbol{r})$ in the vortex core region. In chiral superconductors other than p_--wave superconductor, $\tau_0/\tau(\boldsymbol{r})$ is suppressed in the unitary limit as $1/\tau(\boldsymbol{r}) < 1/\tau_0$, as is seen in Fig. 7. There, p_+, $d_{1\pm}$ and $d_{2\pm}$-wave superconductors show similar $1/\tau_0$-dependence. Around the vortex, $\langle g\rangle_{\boldsymbol{k}} = N(E = 0, \boldsymbol{r})/N_0$ becomes larger, while $|\langle f\rangle_{\boldsymbol{k}}| = |f_s(E = 0, \boldsymbol{r})|$ is not so large and reduces to zero at $r \to 0$ as is seen in Figs. 2 and 4. $\langle f\rangle_{\boldsymbol{k}} = 0$ in $d_{1\pm}$-wave superconductors. Therefore, since dominant contributions of $\langle g\rangle_{\boldsymbol{k}}$ increases at $r \to 0$, $\tau_0/\tau(\boldsymbol{r}) \sim \langle g\rangle_{\boldsymbol{k}}^{-2} = (N(E = 0, \boldsymbol{r})/N_0)^{-2}$ becomes smaller at the vortex core. Since the effectively cleaner vortex core compensates the dirtier outside region, the peak height of $N(E = 0, \boldsymbol{r})$

in the unitary limit may keep almost the same height as in the Born limit in Fig. 5. With increasing $1/\tau_0$ toward dirtier superconductors, $\langle g\rangle_{\boldsymbol{k}}^{-2}$ approaches the normal state value 1, $\tau_0/\tau(\boldsymbol{r})$ approaches 1 both inside and outside of the vortex core, indicating that the difference between the Born and the unitary limits becomes smaller.

On the other hand, in the p_--wave superconductor, $\tau_0/\tau(\boldsymbol{r}) \to 1$ when $r \to 0$ approaching the vortex center. At the vortex core, we find that the odd-frequency s-wave Coooper pair component has the relation $\langle f\rangle_{\boldsymbol{k}}\langle f^\dagger\rangle_{\boldsymbol{k}} = -|f_s(E=0,\boldsymbol{k})|^2$ in $p_\pm$-wave superconductors, whereas $\langle f\rangle_{\boldsymbol{k}}\langle f^\dagger\rangle_{\boldsymbol{k}} = |f_s(E=0,\boldsymbol{k})|^2$ in $d_{2\pm}$-wave ones. In the p_--wave superconductor, $\langle f\rangle_{\boldsymbol{k}} = \langle f^\dagger\rangle_{\boldsymbol{k}} = i|f_s(E=0,\boldsymbol{r})|$ and $\tau_0/\tau(\boldsymbol{r}) = (\langle g\rangle_{\boldsymbol{k}}^2 + \langle f\rangle_{\boldsymbol{k}}\langle f^\dagger\rangle_{\boldsymbol{k}})^{-1} = ((N(E=0,\boldsymbol{r})/N_0)^2 - |f_s(E=0,\boldsymbol{k})|^2)^{-1} \sim 1$ at the vortex center. There, large intensity of $N(E=0,\boldsymbol{r})/N_0$ is almost compensated by the increase of $|f_s(E=0,\boldsymbol{k})|$, seen in Fig. 6. Similar behavior appears also in the negative coherence effect due to the odd-frequency s-wave Coooper pair component in the local NMR relaxation rate T_1^{-1} at the vortex core [48,49]. As is shown in Fig. 5(d), there is small deviation between $N(E=0,\boldsymbol{r})/N_0$ and $|f_s(E=0,\boldsymbol{k})|$ in the unitary limit, so that $(N(E=0,\boldsymbol{r})/N_0)^2 - |f_s(E=0,\boldsymbol{k})|^2 \sim 1$. The result that $\tau_0/\tau(\boldsymbol{r})$ in the unitary limit does not become smaller than that of the Born limit even in the vortex core may be related to the fact that zero-energy LDOS of the vortex bound state is not robust against the nonmagnetic impurity scattering in the unitary limit, while it is robust in the Born limit, as is seen in Fig. 5(a).

To clarify the unconventional behaviors of nonmagnetic impurity scattering effects in the chiral superconductors, we compare results for the chiral superconductors in this section with those for isotropic s-wave superconductors in Appendix.

V. SUMMARY

Based on the self-consistent Eilenberger theory in the vortex lattice, we studied nonmagnetic impurity scattering effects in the vortex states of chiral superconductors, and clarified its dependence on the scattering rates $1/\tau_0$ with a comparison of the Born and unitary limits. To find characters of two chiral d-wave superconductors, $d_{1\pm} = d_{xz} \pm id_{yz}$ and $d_{2\pm} = d_{x^2-y^2} \pm id_{xy}$, in comparison with chiral $p_\pm$-wave superconductors, we calculated the spatial structure of the pair potential and local electronic state in the presence of impurity scattering.

As for the main component $\Delta_1(\boldsymbol{r})$ and the induced opposite chiral component $\Delta_2(\boldsymbol{r})$, reflecting properties of time reversal symmetry breaking, we found that $d_{1\pm}$-wave superconductors have similar spatial structure and the $1/\tau_0$ dependence to those in $p_\pm$-wave superconductors, since both have the same chirality $L_z = \pm 1$. Thus we expect that chirality dependent behaviors induced by $\Delta_2(\boldsymbol{r})$ are similar in $p_\pm$ and $d_{1\pm}$-wave superconductors. However, in $d_{2\pm}$-wave superconductors with $L_z = \pm 2$, since $\Delta_2(\boldsymbol{r})$ shows different spatial behaviors and small amplitude, the difference between d_{2+} and d_{2-}-wave superconductors becomes small in their chirality dependent phenomena.

As for the local electronic states which may be observed by STM experiments, chiral d-wave superconductors show different behavior compared with $p_\pm$-wave superconductors. While zero energy LDOS of vortex bound state is more robust against the nonmagnetic impurity scattering in the p_--wave superconductor in the Born limit, it is rapidly suppressed as a function of $1/\tau_0$ in chiral d-wave superconductors. The rapid suppression occurs even in the p_--wave superconductors in the unitary limit. The differences are due to lack of Majorana properties related to the s-wave Cooper pair amplitude, and one of key features to distinguish between chiral p and d-wave superconductors. Robustness against the impurity scattering effects is also related to the local impurity scattering rate $1/\tau(\boldsymbol{r})$ around a vortex.

These results about the impurity effects in the vortex state will be important in future studies to identify properties of chiral superconductors in candidate materials [8,10–16].

ACKNOWLEDGMENT

This work was supported by JSPS KAKENHI Grants No. 17K05542 and No. 19H00657.

APPENDIX: IMPURITY EFFECTS IN VORTEX STATES OF AN s-WAVE SUPERCONDUCTOR

To understand characteristic behaviors of vortex states in chiral superconductors, we need to see also behaviors in a conventional isotropic s-wave superconductor with $\Delta(\boldsymbol{r},\boldsymbol{p}) = \Delta_s(\boldsymbol{r})$. The spatial structures of the zero-energy LDOS $N(E=0,\boldsymbol{r})/N_0$ and s-wave Cooper pair amplitude $|f_s(E=0,\boldsymbol{r})|$ are, respectively, presented in Figs. 8(a) and 8(b). Outside of the vortex core, the differences between the Born and the unitary limits are very small. Far from the vortex, $N(E=0,\boldsymbol{r})/N_0$ is reduced to a small value, and $|f_s(E=0,\boldsymbol{r})| \to 1$. There, $1/\tau_0$ dependence is very weak, reflecting Anderson theorem that the nonmagnetic impurity scattering effects are absent in the uniform bulk state in an isotropic s-wave superconductor [69,73].

On the other hand, inside of the vortex core we see the $1/\tau_0$ dependence and differences between two limits. As is shown in Fig. 8(c), the peak height of $N(E=0,\boldsymbol{r})/N_0$ at the vortex center $r=0$ decreasing as a function of $1/\tau_0$ is higher in the unitary limit than that in the Born limit [58]. This is contrasted to behaviors of chiral superconductors in Fig. 5, where $N(E=0,\boldsymbol{r})/N_0$ at the vortex center is higher in the Born limit. Approaching vortex, $|f_s(E=0,\boldsymbol{r})|$ increases from 1. And after a peak at finite r, it rapidly decreases towards 0 at $r \to 0$, since $f_s(E=0,\boldsymbol{r})$ has phase winding $w=1$ around a vortex center in an s-wave superconductor. The peak height at finite r decreases, with increasing $1/\tau_0$.

Figure 8(d) shows local scattering rate in the unitary limit. In an s-wave superconductor, $\tau_0/\tau(\boldsymbol{r}) \to 1$ far from the vortex. Approaching the vortex center, $\tau_0/\tau(\boldsymbol{r})$ decreases toward 0 at $r \to 0$. The $1/\tau_0$ dependence is almost negligible. Because of the cleaner vortex core contribution, the impurity scattering effect in the vortex state is weaker in the unitary limit, compared with the case of $\tau_0/\tau(\boldsymbol{r}) = 1$ in the Born limit. This is a reason why the peak height of $N(E=0,\boldsymbol{r})/N_0$ in Fig. 8 is higher in the unitary limit, indicating cleaner than in the Born limit.

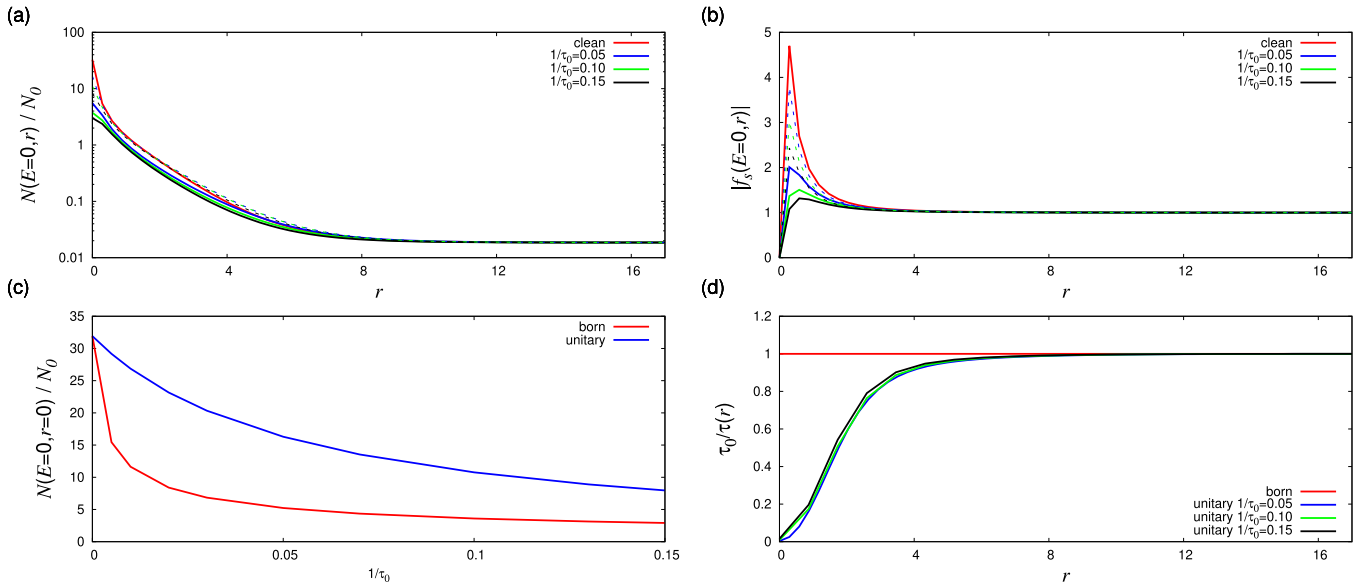

FIG. 8. Vortex states in an isotropic s-wave superconductor for $1/\tau_0 = 0$, 0.05, 0.10, and 0.15 in the Born (solid lines) and the unitary (dashed lines) limits. $T/T_c = 0.5$. $B/B_0 = 0.01$. (a) Zero energy LDOS $N(E = 0, \boldsymbol{r})/N_0$ and (b) s-wave Cooper pair amplitude $|f_s(E = 0, \boldsymbol{r})|$ as a function of radius r along x axis of NNN vortex direction. (c) Peak height of zero-energy LDOS $N(E = 0, r = 0)/N_0$ at the vortex center as a function of $1/\tau_0$ in the Born and unitary limits. (d) Local scattering rate $\tau_0/\tau(\boldsymbol{r})$ from Eq. (9) in the unitary limit as a function of r for $1/\tau_0 = 0.05$, 0.10, and 0.15. In the Born limit, $\tau_0/\tau(\boldsymbol{r}) = 1$.

[1] A. J. Leggett, A theoretical description of the new phases of liquid ^{3}He, Rev. Mod. Phys. **47**, 331 (1975).

[2] A. P. Mackenzie and Y. Maeno, The superconductivity of Sr_2RuO_4 and the physics of spin-triplet pairing, Rev. Mod. Phys. **75**, 657 (2003).

[3] Y. Maeno, S. Kittaka, T. Nomura, S. Yonezawa, and K. Ishida, Evaluation of Spin-Triplet Superconductivity in Sr_2RuO_4, J. Phys. Soc. Jpn. **81**, 011009 (2012).

[4] G. M. Luke, Y. Fudamoto, K. M. Kojima, M. L. Larkin, J. Merrin, B. Nachumi, Y. J. Uemura, Y. Maeno, Z. Q. Mao, Y. Mori, H. Nakamura, and M. Sigrist, Time-reversal symmetry-breaking superconductivity in Sr_2RuO_4, Nature (London) **394**, 558 (1998).

[5] J. Xia, Y. Maeno, P. T. Beyersdorf, M. M. Fejer, and A. Kapitulnik, High Resolution Polar Kerr Effect Measurements of Sr_2RuO_4: Evidence for Broken Time-Reversal Symmetry in the Superconducting State, Phys. Rev. Lett. **97**, 167002 (2006).

[6] K. Ishida, H. Mukuda, Y. Kitaoka, K. Asayama, Z. Q. Mao, Y. Mori, and Y. Maeno, Spin-triplet superconductivity in Sr_2RuO_4 identified by ^{17}O Knight shift, Nature (London) **396**, 658 (1998).

[7] J. A. Duffy, S. M. Hayden, Y. Maeno, Z. Mao, J. Kulda, and G. J. McIntyre, Polarized-Neutron Scattering Study of the Cooper-Pair Moment in Sr_2RuO_4, Phys. Rev. Lett. **85**, 5412 (2000).

[8] A. Pustogow, Y. Luo, A. Chronister, Y.-S. Su, D. A. Sokolov, F. Jerzembeck, A. P. Mackenzie, C. W. Hicks, N. Kikugawa, S. Raghu, E. D. Bauer, and S. E. Brown, Constraints on the superconducting order parameter in Sr_2RuO_4 from oxygen-17 nuclear magnetic resonance, Nature (London) **574**, 72 (2019).

[9] K. Ishida, M. Manago, K. Kinjo, and Y. Maeno, Reduction of the ^{17}O Knight Shift in the Superconducting State and the Heat-up Effect by NMR Pulses on Sr_2RuO_4, J. Phys. Soc. Jpn. **89**, 034712 (2020).

[10] G. M. Luke, A. Keren, L. P. Le, W. D. Wu, Y. J. Uemura, D. A. Bonn, L. Taillefer, and J. D. Garrett, Muon Spin Relaxation in UPt_3, Phys. Rev. Lett. **71**, 1466 (1993).

[11] E. R. Schemm, W. J. Gannon, C. M. Wishne, W. P. Halperin, and A. Kapitulnik, Observation of broken time-reversal symmetry in the heavy-fermion superconductor UPt_3, Science **345**, 190 (2014).

[12] K. E. Avers, W. J. Gannon, S. J. Kuhn, W. P. Halperin, J. A. Sauls, L. DeBeer-Schmitt, C. D. Dewhurst, J. Gavilano, G. Nagy, U. Gasser, and M. R. Eskildsen, Broken time-reversal symmetry in the topological superconductor UPt_3, Nat. Phys. **16**, 531 (2020).

[13] S. Ran, I-L. Liu, Y. S. Eo, D. J. Campbell, P. M. Neves, W. T. Fuhrman, S. R. Saha, C. Eckberg, H. Kim, D. Graf, F. Balakirev, J. Singleton, J. Paglione, and N. P. Butch, Extreme magnetic field-boosted superconductivity, Nat. Phys. **15**, 1250 (2019).

[14] E. R. Schemm, R. E. Baumbach, P. H. Tobash, F. Ronning, E. D. Bauer, and A. Kapitulnik, Evidence for broken time-reversal symmetry in the superconducting phase of URu_2Si_2, Phys. Rev. B **91**, 140506(R) (2015).

[15] P. K. Biswas, H. Luetkens, T. Neupert, T. Stürzer, C. Baines, G. Pascua, A. P. Schnyder, M. H. Fischer, J. Goryo, M. R. Lees, H. Maeter, F. Brückner, H.-H. Klauss, M. Nicklas, P. J. Baker, A. D. Hillier, M. Sigrist, A. Amato, and D. Johrendt, Evidence for superconductivity with broken time-reversal symmetry in locally noncentrosymmetric SrPtAs, Phys. Rev. B **87**, 180503(R) (2013).

[16] H. Ueki, R. Tamura, and J. Goryo, Possibility of chiral d-wave state in the hexagonal pnictide superconductor SrPtAs, Phys. Rev. B **99**, 144510 (2019).

[17] C. Caroli, P. G. de Gennes, and J. Matricon, Bound Fermion States on a Vortex Line in a Type II Superconductor, Phys. Lett. **9**, 307 (1964).

[18] F. Gygi and M. Schlüter, Electronic tunneling into an isolated vortex in a clean type-II superconductor, Phys. Rev. B **41**, 822 (1990).

[19] F. Gygi and M. Schlüter, Self-consistent electronic structure of a vortex line in a type-II superconductor, Phys. Rev. B **43**, 7609 (1991).

[20] H. F. Hess, R. B. Robinson, R. C. Dynes, J. M. Valles, and J. V. Waszczak, Scanning-Tunneling-Microscope Observation of the Abrikosov Flux Lattice and the Density of States Near and Inside a Fluxoid, Phys. Rev. Lett. **62**, 214 (1989).

[21] H. F. Hess, R. B. Robinson, and J. V. Waszczak, Vortex-Core Structure Observed with a Scanning Tunneling Microscope, Phys. Rev. Lett. **64**, 2711 (1990).

[22] H. F. Hess, R. B. Robinson, and J. V. Waszczak, Scanning-Tunneling-Microscopy Study of Distortion and Instability of Inclined Flux-Line-Lattice Structures in the Anisotropic Superconductor 2H-$NbSe_2$, Phys. Rev. Lett. **69**, 2138 (1992).

[23] Ch. Renner, A. D. Kent, Ph. Niedermann, Ø. Fischer, and F. Lévy, Scanning Tunneling Spectroscopy of a Vortex Core from the Clean to the Dirty Limit, Phys. Rev. Lett. **67**, 1650 (1991).

[24] Ø. Fischer, M. Kugler, I. Maggio-Aprile, C. Berthod, and Ch. Renner, Scanning tunneling spectroscopy of high-temperature superconductors, Rev. Mod. Phys. **79**, 353 (2007).

[25] M. Ichioka, A. Hasegawa, and K. Machida, Vortex lattice effects on low-energy excitations in d-wave and s-wave superconductors, Phys. Rev. B **59**, 184 (1999).

[26] N. Schopohl and K. Maki, Quasiparticle spectrum around a vortex line in a d-wave superconductor, Phys. Rev. B **52**, 490 (1995).

[27] M. Ichioka, N. Hayashi, N. Enomoto, and K. Machida, Vortex structure in d-wave superconductors, Phys. Rev. B **53**, 15316 (1996).

[28] M. Ichioka, A. Hasegawa, and K. Machida, Field dependence of the vortex structure in d-wave and s-wave superconductors, Phys. Rev. B **59**, 8902 (1999).

[29] N. Hayashi, M. Ichioka, and K. Machida, Star-Shaped Local Density of States around Vortices in a Type-II Superconductor, Phys. Rev. Lett. **77**, 4074 (1996).

[30] N. Hayashi, M. Ichioka, and K. Machida, Effects of gap anisotropy upon the electronic structure around a superconducting vortex, Phys. Rev. B **56**, 9052 (1997).

[31] H. Nishimori, K. Uchiyama, S. Kaneko, A. Tokura, H. Takeya, K. Hirata, and N. Nishida, First observation of the fourfold-symmetric and quantum regime vortex core in YNi_2B_2C by scanning tunneling microscopy and spectroscopy, J. Phys. Soc. Jpn. **73**, 3247 (2004).

[32] S. Kaneko, K. Matsuba, M. Hafiz, K. Yamasaki, E. Kalizaki, N. Nishida, H. Takeya, K. Hirata, T. Kawakami, T. Mizushima, and K. Machida, Quantum limiting behaviors of a vortex core in an anisotropic gap superconductor, J. Phys. Soc. Jpn. **81**, 063701 (2012).

[33] Y. Nagai, Y. Kato, N. Hayashi, K. Yamauchi, and H. Harima, Calculated positions of point nodes in the gap structure of the borocarbide superconductor YNi_2B_2C, Phys. Rev. B **76**, 214514 (2007).

[34] R. Heeb and D. F. Agterberg, Ginzburg-Landau theory for a p-wave Sr_2RuO_4 superconductor: Vortex core structure and extended London theory, Phys. Rev. B **59**, 7076 (1999).

[35] M. Ichioka, and K. Machida, Field dependence of the vortex structure in chiral p-wave superconductors, Phys. Rev. B **65**, 224517 (2002).

[36] M. Ichioka, Y. Matsunaga, and K. Machida, Magnetization process in a chiral p-wave superconductor with multidomains, Phys. Rev. B **71**, 172510 (2005).

[37] M. Matsumoto and M. Sigrist, Chiral optical absorption by a vortex in $p_x \pm ip_y$-wave superconductor, J. Phys. Soc. Jpn. **68**, 724 (1999).

[38] M. Matsumoto and R. Heeb, Vortex charging effect in a chiral $p_x \pm ip_y$-wave superconductor, Phys. Rev. B **65**, 014504 (2001).

[39] M. Takigawa, M. Ichioka, K. Machida, and M. Sigrist, Vortex structure in chiral p-wave superconductors, Phys. Rev. B **65**, 014508 (2001).

[40] N. Read and D. Green, Paired states of fermions in two dimensions with breaking of parity and time-reversal symmetries and the fractional quantum Hall effect, Phys. Rev. B **61**, 10267 (2000).

[41] D. A. Ivanov, Non-Abelian Statistics of Half-Quantum Vortices in p-Wave Superconductors, Phys. Rev. Lett. **86**, 268 (2001).

[42] T. Mizushima, M. Ichioka, and K. Machida, Role of the Majorana Fermion and the Edge Mode in Chiral Superfluidity near a p-Wave Feshbach Resonance, Phys. Rev. Lett. **101**, 150409 (2008).

[43] Y. Tanaka, M. Sato, and N. Nagaosa, Symmetry and topology in superconductors: Odd-frequency pairing and edge states, J. Phys. Soc. Jpn. **81**, 011013 (2012).

[44] T. Daino, M. Ichioka, T. Mizushima, and Y. Tanaka, Odd-frequency Cooper-pair amplitude around a vortex core in a chiral p-wave superconductor in the quantum limit, Phys. Rev. B **86**, 064512 (2012).

[45] N. Hayashi and Y. Kato, Nuclear magnetic relaxation rate in the vortex state of a chiral p-wave superconductor, Physica C **388-389**, 513 (2003).

[46] N. Hayashi and Y. Kato, Interplay Between Vorticity and Chirality inside the vortex core in chiral p-wave superconductors, J. Low Temp. Phys. **131**, 893 (2003).

[47] Y. Kato and N. Hayashi, Physics of vortex core in chiral p-wave superconductor, Physica C **388-389**, 519 (2003).

[48] K. K. Tanaka, M. Ichioka, and S. Onari, Site-selective NMR for odd-frequency Cooper pairs around vortex in chiral p-wave superconductors, Phys. Rev. B **93**, 094507 (2016).

[49] K. K. Tanaka, M. Ichioka, and S. Onari, Local NMR relaxation rates T_1^{-1} and T_2^{-1} depending on the d-vector symmetry in the vortex state of chiral and helical p-wave superconductors, Phys. Rev. B **97**, 134507 (2018).

[50] Y. Kato and N. Hayashi, Kramer-Pesch effect in chiral p-wave superconductors, J. Phys. Soc. Jpn. **70**, 3368 (2001).

[51] Y. Tanuma, N. Hayashi, Y. Tanaka, and A. A. Golubov, Model for Vortex-Core Tunneling Spectroscopy of Chiral p-Wave Superconductors via Odd-Frequency Pairing States, Phys. Rev. Lett. **102**, 117003 (2009).

[52] G. Eilenberger, Transformation of Gorkov's equation for type II superconductors into transport-like equations, Z. Phys. **214**, 195 (1968).

[53] U. Klein, Microscopic calculations on the vortex state of type II superconductors, J. Low Temp. Phys. **69**, 1 (1987).

[54] P. Miranović, M. Ichioka, and K. Machida, Effects of nonmagnetic scatterers on the local density of states around a vortex in *s*-wave superconductors, Phys. Rev. B **70**, 104510 (2004).

[55] K. K. Tanaka, M. Ichioka, N. Nakai, and K. Machida, Knight shift spectrum in vortex states in *s*- and *d*-wave superconductors on the basis of Eilenberger theory, Phys. Rev. B **89**, 174504 (2014).

[56] E. V. Thuneberg, J. Kurkijärvi, and D. Rainer, Elementary-flux-pinning potential in type-II superconductors, Phys. Rev. B **29**, 3913 (1984).

[57] Y. Kato, Phase-sensitive impurity effects in vortex core of moderately clean chiral superconductors, J. Phys. Soc. Jpn. **69**, 3378 (2000).

[58] M. Eschrig, D. Rainer, and J. A. Sauls, *Vortices in Unconventional Superconductors and Superfluids*, edited by R. P. Huebener, N. Schopohl, and G. E. Volovik (Springer, Heidelberg, 2002), p. 175.

[59] Y. Sera, T. Ueda, H. Adachi, and M. Ichioka, Relation of superconducting pairing symmetry and non-magnetic impurity effects in vortex states, Symmetry **12**, 175 (2020).

[60] Y. Hashitani, K. K. Tanaka, H. Adachi, and M. Ichioka, Variation of zero-energy density of states of a *d*-wave superconductor in a rotating in-plane magnetic field: Effect of nonmagnetic impurities, Phys. Rev. B **101**, 060501(R) (2020).

[61] N. Hayashi and Y. Kato, Elementary vortex pinning potential in a chiral *p*-wave superconductor, Phys. Rev. B **66**, 132511 (2002).

[62] N. Hayashi, Y. Kato, and M. Sigrist, Impurity effect on Kramer-Pesch core shrinkage in *s*-wave vortex and chiral *p*-wave vortex, J. Low Temp. Phys. **139**, 79 (2005).

[63] J. A. Sauls and M. Eschrig, Vortices in chiral, spin-triplet superconductors and superfluids, New J. Phys. **11**, 075008 (2009).

[64] T. M. Riseman, P. G. Kealey, E. M. Forgan, A. P. Mackenzie, L. M. Galvin, A. W. Tyler, S. L. Lee, C. Ager, D. Mck. Paul, C. M. Aegerter, R. Cubitt, Z. Q. Mao, T. Akima, and Y. Maeno, Observation of a square flux-line lattice in the unconventional superconductor Sr_2RuO_4, Nature (London) **396**, 242 (1998); **404**, 629(E) (2000).

[65] D. F. Agterberg, Vortex Lattice Structures of Sr_2RuO_4, Phys. Rev. Lett. **80**, 5184 (1998).

[66] T. Kita, Vortex States of E_u Model for Sr_2RuO_4, Phys. Rev. Lett. **83**, 1846 (1999).

[67] P. Miranović and K. Machida, Thermodynamics and magnetic field profiles in low-κ type-II superconductors, Phys. Rev. B **67**, 092506 (2003).

[68] M. Ichioka, V. G. Kogan, and J. Schmalian, Locking of length scales in two-band superconductors, Phys. Rev. B **95**, 064512 (2017).

[69] A. A. Abrikosov and L. P. Gor'kov, On the Theory of Superconducting Alloys I. The Electrodynamics of Alloys at Absolute Zero, Zh. Eksp. Teor. Fiz. **35**, 1558 (1958); Sov. Phys. JETP **8**, 1090 (1959).

[70] V. Ambegaokar, The Green's function method, in *Superconductivity*, edited by R. D. Parks (Marcel Dekker, New York, 1969), Chap. 5.

[71] N. R. Werthamer, The Ginzburg-Landau equation and their extensions, in *Superconductivity*, edited by R. D. Parks (Marcel Dekker, New York, 1969), Chap. 6.

[72] P. G. de Gennes, *Superconductivity of Metals and Alloys* (Benjamin, New York, 1966), Chap. 7.

[73] P. W. Anderson, Theory of dirty superconductors, J. Phys. Chem. Solids **11**, 26 (1959).